Sixth International Symposium on Turbulence and Shear Flow Phenomena
Seoul, Korea, 22-24 June 2009

INVESTIGATION OF ENSTROPHY PRODUCTION IN THE FAR FIELD OF AN AXISYMMETRIC TURBULENT JET

Oliver R.H. Buxton
Department of Aeronautics,
Imperial College London
Prince Consort Road, London, U.K.
o.buxton07@imperial.ac.uk

Bharathram Ganapathisubramani
Department of Aeronautics,
Imperial College London
Prince Consort Road, London, U.K.
g.bharath@imperial.ac.uk

ABSTRACT

Cinematographic stereoscopic particle image velocimetry (PIV) was used to extract three dimensional velocity and velocity gradient information on fine scale turbulence in the far field of an axisymmetric jet. The Reynolds number based on the Taylor micro-scale was 150. The interaction between strain and rotation in the production of enstrophy is examined by observing the alignment of the vorticity vector with the principal axes of the rate of strain tensor. The vorticity vector is generally aligned with the intermediate strain rate, consistent with various other studies in the literature. However, in regions of intense vortex stretching, the vorticity vector shows a tendency to align with the extensive strain rate. These regions of intense vortex stretching are found in the vicinity of locally swirling regions (i.e. regions where the local velocity gradient tensor has a complex conjugate pair of eigenvalues). Moreover, instantaneous iso-surfaces of intense vortex stretching regions show the presence of "sheet-like" structures that are characterised by positive (extensive) intermediate strain rate. Statistical results based on probability distributions also confirm this behaviour. A possible physical mechanism is proposed whereby enstrophy is produced in weakly swirling regions and subsequently evolve under the action of the strain rate tensor to form "tube" or "worms".

INTRODUCTION

The velocity gradient tensor ($D_{ij} = \partial u_i/\partial x_j$) can be written as the sum of the symmetric rate of strain tensor, $S_{ij} = (\partial u_i/\partial x_j + \partial u_j/\partial x_i)/2$ and the skew-symmetric rotation tensor, $\Omega_{ij} = (\partial u_i/\partial x_j - \partial u_j/\partial x_i)/2$. The interaction between strain and rotation is fundamental in characterising the nature of three dimensional turbulence, especially to the production and evolution of enstrophy, as can be seen in equation 1.

$$\boldsymbol{\omega} \cdot \frac{\mathrm{D}\boldsymbol{\omega}}{\mathrm{D}t} = \boldsymbol{\omega} \cdot [(\boldsymbol{u} \cdot \nabla)\omega] + \nu \boldsymbol{\omega} \cdot \nabla^2 \boldsymbol{\omega} \qquad (1)$$

$$\text{where,} \quad \boldsymbol{\omega} \cdot [(\boldsymbol{u} \cdot \nabla)\omega] = \omega_i S_{ij} \omega_j$$

It can be seen that equation 1 consists of an enstrophy production term ($\omega_i S_{ij} \omega_j$) and a viscous dissipation term. Furthermore it can be shown that the magnitude of the production term $|S_{ij}\omega_j| = \omega \left[s_i^2 (\hat{\boldsymbol{e}}_{\boldsymbol{i}} \cdot \hat{\boldsymbol{\omega}})^2 \right]^{1/2}$ (Hamlington et al., 2008) depends on the strain rate eigenvalues s_i, the vorticity magnitude $\omega = (\omega_i \omega_i)^{1/2}$, and on the cosines of the alignment angle between the unit vorticity vector $\hat{\boldsymbol{\omega}}$ and the unit strain rate eigenvectors $\hat{\boldsymbol{e}}_{\boldsymbol{i}}$, thus highlighting the interaction between strain and rotation. The preponderance of the vorticity vector to be aligned with the intermediate strain rate eigenvector was first observed in a numerical study by Ashurst et al. (1987) and was subsequently confirmed experimentally by Tsinober et al. (1992). Recently, Buxton and Ganapathisubramani (2009) examined the alignment of the swirling eigenvector (defined as the real eigenvector for regions in which the velocity gradient tensor has a real and complex conjugate pair of eigenvectors) and the eigenvectors of the rate of strain tensor. They observed that the swirling eigenvector tends to preferentially align itself to the extensive strain rate eigenvector, particularly in regions for which the local swirling was weak and showed that weakly swirling regions also tended to coincide with a negative intermediate strain rate. The authors suggested a mechanism in which weakly swirling regions of vorticity are extended, by virtue of the fact that they are aligned to the extensive strain rate, whilst tending to form the coherent strongly swirling, high enstrophy "worms" observed in fine scale turbulent flows (Siggia, 1981; Kerr, 1985; Ashurst et al., 1987).

Much of the earlier work pertaining to the small-scale turbulent motions compared statistical estimates, such as probability density functions (*pdf*s), skewness and flatness of gradient quantities such as vorticity and dissipation. A review of such work can be found in Sreenivasan and Antonia (1997). However, in order to reveal the instantaneous topology of these vorticity and dissipation fields three dimensional velocity and velocity gradient information is required. This three dimensional information has become available through direct numerical simulation (DNS) studies (She et al., 1990; Vincent and Meneguzzi, 1991; Jiménez et al.,1993; Vincent and Meneguzzi, 1994; da Silva and Pereira, 2008). Cinematographic stereoscopic particle image velocimetry (PIV) has also been employed, recently, to gather this three dimensional velocity and velocity gradient data experimentally (Ganapathisubramani et al., 2007; Ganapathisubramani et al., 2008). This study will use data that has been gathered by cinematographic stereoscopic PIV to examine the production and evolution of enstrophy within the far field of an axisymmetric turbulent jet. Particular emphasis will

be given to the interaction between straining regions and swirling ones (swirling regions are defined as those regions where the velocity gradient tensor has a complex pair of eigenvalues), through the alignment of the vorticity vector and swirling eigenvector with the principal axes of the strain rate tensor, and the topological evolution of the flow as characterised by the intermediate strain rate.

EXPERIMENTAL METHODS AND TECHNIQUES

The data used in this study was obtained by Ganapathisubramani et al. (2007). The experiments were performed in the far field of a co-flowing axisymmetric turbulent jet of air, as described in Ganapathisubramani et al. (2007). The facility is 920 mm wide by 920 mm long and 1170 mm high and was constructed from aluminium. The axisymmetric jet exhausted into a mild co-flow of air from a pipe of circular cross section (diameter, $D = 26$ mm), located at the centre of the co-flow facility. Tsurikov (2003), who developed the experimental facility, acquired velocity profiles using hot film probes and documented the presence of a fully developed turbulent pipe flow at the jet exit. Additionally, Tsurikov (2003) performed further hot film and PIV measurements in various azimuthal planes to ensure that the jet remained axisymmetric at exit. The jet velocity was $U_0 = 3$ m/s and the co-flow velocity was $U_\infty = 0.15$ m/s. The boundary layer on the outside of the jet, due to the co-flow, was laminar with an estimated thickness of 11 mm near the jet exit. Information regarding the characterisation of the jet's flow field in addition to the design and construction of the facility is presented in Tsurikov (2003).

The relevant length scales at the measurement location are: jet half width ($\delta_{1/2}$) = 126 mm, Taylor micro-scale (λ) = 13.8 mm, Kolmogorov scale ($\eta = \left(\nu^3/\bar{\epsilon}\right)^{1/4}$) = 0.45 mm, where the mean rate of dissipation ($\bar{\epsilon}$) was calculated from the experimental data. The Reynolds number based on jet exit velocity and diameter, Re_D, = 5100 and the Reynolds number based on the Taylor micro-scale, Re_λ, $\approx$ 150.

Cinematographic stereoscopic PIV measurements were performed in the "end view" plane ($x_2 - x_3$) at a downstream axial location of $x_1 = 32D$ (N.B. in this study, x_1 is the axial direction and x_2 and x_3 are the two orthogonal radial directions). The cinematographic PIV system consisted of a Nd:YLF laser with output wavelength of 527 nm and a pair of high-framing rate 1024×1024 pixel resolution CMOS cameras that were operated at a rate of 2 kHz. The particles were seeded into the co-flow and subsequently entrained by the developing turbulent jet. The seed particles were illuminated by a laser sheet of thickness $\approx$ 1 mm and the scattered light was captured by the two CMOS cameras in stereoscopic arrangement oriented at an angle of 30° to the axis of the jet. Cinematographic images were captured for a duration of 1 s, corresponding to a total of 2000 frames and 2 GB of data for each experimental run. The vector fields were computed by correlating successive particle images in the movie sequence ($\Delta t = 500$ μs, since the frequency of image acquisition was 2 kHz). The resulting vectors from each camera were then combined to compute all three velocity components. The resolution of the resulting stereoscopic vector fields is approximately $3\eta \times 3\eta$ (1.35×1.35 mm^2) and successive vectors are separated by 1.5η (due to 50% overlap). The total field size is $160\eta \times 160\eta$ (76×76 mm^2).

In order to reduce the noise on quantities calculated from first order velocity gradients (e.g. vorticity) and products of first order quantities (e.g. $\omega_i S_{ij} \omega_j$) the velocity field data was filtered. A Gaussian smoothing filter with filter width

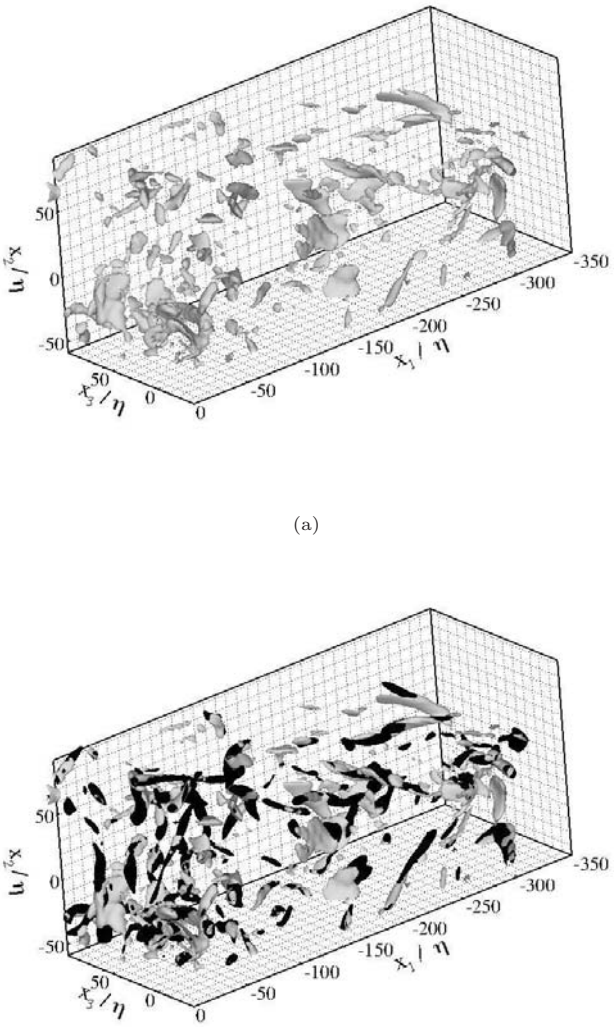

Figure 1: (a) Isosurfaces of enstrophy production rate, $\omega_i S_{ij} \omega_j = 2 \times 10^5$ s^{-3}. (b) Isosurfaces of $\omega_i S_{ij} \omega_j = 2 \times 10^5$ s^{-3} (white) and isosurfaces of local swirling strength, $\lambda_{ci} = 75$ s^{-1} (black). Taylor's hypothesis is used to construct the volume from 200 instantaneous PIV frames. The axes are scaled by the Kolmogorov length scale, η.

$\lambda_f = 6\eta$ (i.e. full width of the Gaussian smoothing function at $1/e^2 = 6\eta$) was used to filter the data along all three directions. Additional information regarding the experimental setup and validation can be found in Ganapathisubramani et al. (2007) and Ganapathisubramani et al. (2008).

INSTANTANEOUS RESULTS

The term $\omega_i S_{ij} \omega_j$ in equation 1 is the enstrophy production rate, and can be either positive (corresponding to vortex stretching regions) or negative (corresponding to vortex compression regions). Higher Reynolds number flows have been shown to favour vortex stretching (i.e. production of enstrophy) to vortex compression (Mullin and Dahm, 2006). Figure 1(a) shows instantaneous isosurfaces of regions of strong vortex stretching ($\omega_i S_{ij} \omega_j > 2 \times 10^5$ s^{-3}). Taylor's

hypothesis was used to produce the volume displayed in figures 1(a) and (b) from 200 instantaneous PIV frames (please see Ganapathisubramani et al., 2007, 2008, for further details on volume reconstruction). The figure shows that the regions of intense vortex stretching appear to be in the form of sheets. Visualising these iso-surfaces from other perspective directions (figures not shown) reinforce this point. The total number of data points that exceed this strong vortex stretching threshold occupy only 5.5 % of the total number of data points, yet they are responsible for 44.7 % of the total enstrophy production (i.e. $\omega_i S_{ij} \omega_j > 0$) making these strong vortex stretching regions extremely significant.

Vorticity is comprised of both straining and swirling regions, the interaction between these two being of great significance in the characterisation of three dimensional turbulence. It is thus important to be able to identify swirling regions from straining ones. Local swirling is defined as being the presence of locally circular/spiral streamlines. It can be shown that when the local velocity gradient tensor has one real (λ_r) and a complex conjugate pair of eigenvalues ($\lambda_{cr} \pm i\lambda_{ci}$) this criterion is met (Jeong and Hussain, 1995). Furthermore the magnitude of the imaginary part of the complex conjugate pair of eigenvalues, λ_{ci}, is a measure of the local swirling strength. Regions of intense, swirling enstrophy have been observed to be topologically "tube-like" (e.g. Jiménez et al., 1993). Figure 1(b) shows intensely swirling regions, in black, ($\lambda_{ci} > 75$ s^{-1}) together with iso-surfaces of intense vortex stretching regions. The figure clearly reveals the "tube-like" nature of these high enstrophy, intensely swirling structures, consistent with other studies in the literature. The strongly swirling regions are also observed to be situated within the regions of strong vortex stretching. However, the intense vortex stretching regions are not exclusive to the strongly swirling regions. In fact, the vortex stretching regions are much larger in size compared to vortex "tubes"/"worms".

Figure 2 displays isosurfaces of $\omega_i S_{ij} \omega_j = -1.5 \times 10^5$ s^{-3}, and hence shows regions of intense vortex compression. There is a far wider range of topologies for these regions than for the high enstrophy producing regions of figure 1, with the structure of these regions tending to be less well defined. This is consistent with the results of Ganapathisubramani et al. (2008) who found that large negative values of s_2 appear "spotty". This also suggests that vortex compression regions coincide with areas of negative s_2.

STATISTICAL RESULTS

Higher Reynolds number flows have been observed to favour vortex stretching ($\omega_i S_{ij} \omega_j > 0$), over vortex compression ($\omega_i S_{ij} \omega_j < 0$) (Tsinober et al., 1997; Mullin and Dahm, 2006). Figure 3 shows the probability density function, *pdf*, for the enstrophy production rate ($\omega_i S_{ij} \omega_j$) normalised by $(\nu/\eta^2)^3$, where ν is the kinematic viscosity and η is the Kolmogorov length scale, plotted on a semi-logarithmic scale.

The figure shows that there is a significant peak close to zero but that the *pdf* is not symmetric. The positive tail is "fatter" than the negative one, indicating an overall tendency for the enstrophy production rate to be positive, or favouring a source term to a sink term. This is in agreement with the fact that vortex stretching is observed to be prevalent over vortex compression in turbulent flows. The shape of this *pdf* agrees well with the dual plane stereo PIV study of Mullin and Dahm (2006).

Figure 4 shows a joint *pdf* between the relative magnitude of local swirling strength ($\lambda_{ci}/\bar{\lambda}_{ci}$, where $\bar{\lambda}_{ci}$ is the

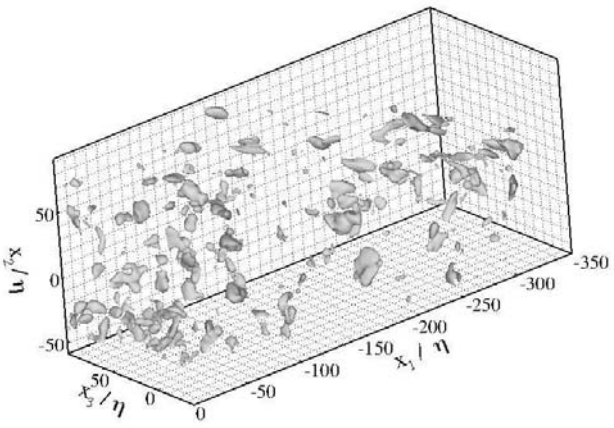

Figure 2: Isosurfaces of enstrophy production rate, $\omega_i S_{ij} \omega_j = -1.5 \times 10^5$ s^{-3}. Taylor's hypothesis is used to construct the volume from 200 instantaneous PIV frames. The axes are scaled by the Kolmogorov length scale, η.

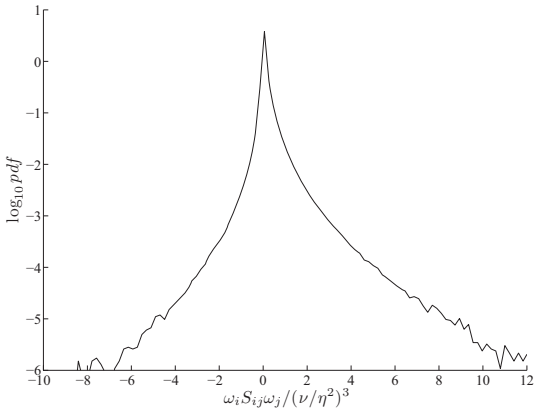

Figure 3: Probability density function (*pdf*) for the enstrophy production rate ($\omega_i S_{ij} \omega_j$) normalised by $(\nu/\eta^2)^3$, where ν is the kinematic viscosity and η is the Kolmogorov length scale. N.B. the ordinate axis is logarithmic.

mean value of swirling strength) and the logarithm of the enstrophy production rate ($\omega_i S_{ij} \omega_j / (\nu/\eta^2)^3$) for regions where the enstrophy production rate is positive (vortex stretching). A horizontal dashed line that represents the mean value of the local swirling strength, $\bar{\lambda}_{ci} = 21.2$ s^{-1}, is marked on the figure. The figure shows that a large proportion of enstrophy production takes place in weakly swirling regions of the turbulent flow. The data indicates that 35.9 % of all the enstrophy producing data points ($\omega_i S_{ij} \omega_j > 0$) are weakly swirling ($0 < \lambda_{ci} < \bar{\lambda}_{ci}$) and 40.5% of these enstrophy producing data points are straining (i.e. there is no local swirling, $\lambda_{ci} = 0$). These two regions account for 19.1% and 22.2% of the total enstrophy production respectively. A threshold value of $\omega_i S_{ij} \omega_j > 2.0 \times 10^5$ s^{-3} is used to illustrate the behaviour of strongly vortex stretching regions. As mentioned previously, only 5.5 % of all the enstrophy producing data points exceed this threshold (marked onto the figure with a vertical dashed line), yet they account for 44.7 % of the total enstrophy production. Of these strong

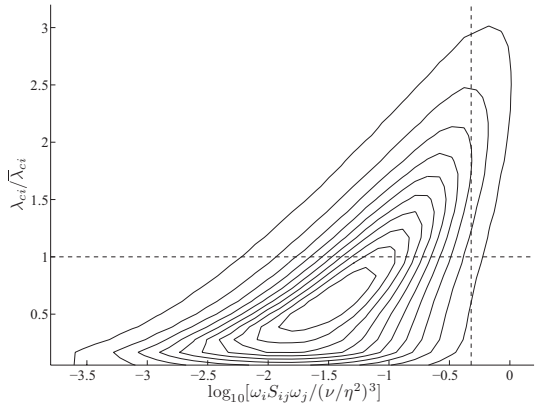

Figure 4: Joint probability density function (*pdf*) for local swirling strength (λ_{ci}) and the logarithm of the enstrophy production rate ($\omega_i S_{ij}\omega_j$) for regions in which this term is positive (i.e. enstrophy is being produced). The outer contour is at level 0.045 and the inner contour at level 0.45. The separation between successive contour levels is 0.045. The mean value of local swirling strength, $\bar{\lambda}_{ci} = 21.2$ s^{-1} is marked on the figure as the horizontal dashed line and the vertical dashed line represents the threshold value of $\omega_i S_{ij}\omega_j = 2.0 \times 10^5$ s^{-3}.

vortex stretching data points, 86.2 % exhibit local swirling, of which the mean value is 50.5 s^{-1}.

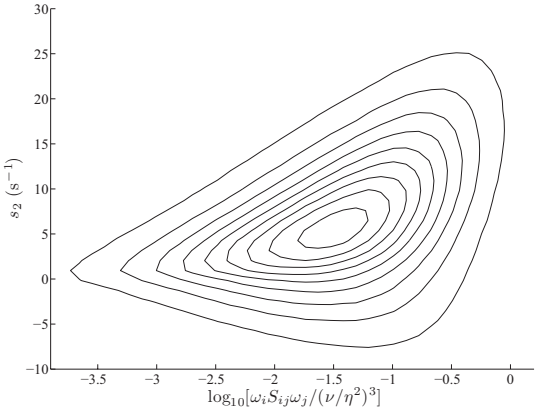

Figure 5: Joint probability density function (*pdf*) between the intermediate strain rate (s_2) and the logarithm of the enstrophy production rate ($\omega_i S_{ij}\omega_j$) for regions in which this term was positive (i.e. enstrophy is being produced). The outer contour is at level 0.0035 and the inner contour at level 0.035. The separation between successive contour levels is 0.0035.

Figure 5 shows the joint probability density function between the intermediate strain rate (s_2) and the logarithm of the enstrophy production rate ($\omega_i S_{ij}\omega_j/(\nu/\eta^2)^3$), for regions in which this term was positive (i.e. enstrophy is being produced). The intermediate strain rate is responsible for determining the local topological evolution of a fluid element. The intermediate strain rate is bounded by the extensive strain rate (s_1) and the compressive strain rate (s_3), and may therefore be either positive (extensive) or negative (compressive). An element subjected to two principal orthogonal axes of extension, and one of compression ($s_2 > 0$) will tend to form "sheet-like" topology, whereas an element subjected to two orthogonal axes of compression, and one of extension ($s_2 < 0$) will tend to form "tube-like" topology. It can be seen that the contours of the joint *pdf* extend further in the positive s_2 domain than the negative, and that they slope towards positive s_2 for more strongly vortex stretching regions. This suggests that the intense vortex stretching regions coincide with relatively large positive values of s_2. It can therefore be concluded that enstrophy producing regions tend to be "sheet-forming", due to the intermediate strain rate tending to be extensive, especially for the regions of strong vortex stretching. This statistical observation is in agreement with the instantaneous observation of "sheet-like" topology for the strong vortex stretching regions of figure 1.

It was shown previously that the magnitude of the enstrophy production term depends upon the cosine of the alignment angle between the vorticity vector and the eigenvectors of the strain rate tensor. Ashurst et al. (1987) first noted that the vorticity vector is preferentially aligned with the intermediate strain rate eigenvector ($\boldsymbol{e_2}$). This has subsequently been confirmed by numerical and experimental studies (Tsinober et al., 1997 among others). In contrast, the alignment between the vorticity vector and the extensive strain rate eigenvector ($\boldsymbol{e_1}$) has been observed to be random, producing a flat *pdf*.

Figure 6 shows probability density functions (*pdf*s) for the cosine of the alignment angle between the vorticity vector ($\boldsymbol{\omega}$) and the extensive and intermediate strain rates ($\boldsymbol{e_1}$ and $\boldsymbol{e_2}$) respectively. The solid lines in figure 6(a) and (b) are *pdf*s constructed from all the available data points whereas the dashed lines represent *pdf*s generated solely from regions in which the enstrophy production rate is positive, i.e. vortex stretching is taking place. The preponderance for the vorticity vector to be aligned with the intermediate strain rate eigenvector can be seen from the solid line *pdf* in figure 6(b), as there is a clear peak at $\hat{\boldsymbol{e_2}} \cdot \hat{\boldsymbol{\omega}} = 1$. Conversely the random alignment between the extensive strain rate eigenvector and the vorticity vector can also be observed from the solid line *pdf* of figure 6(a). By contrast the dashed line *pdf* shows a peak at $\hat{\boldsymbol{e_1}} \cdot \hat{\boldsymbol{\omega}} = 1$ indicating that the vorticity vector preferentially aligns with the extensive strain rate in regions for which the enstrophy production rate is positive. There is, however, relatively little difference between the solid and dashed line *pdf*s of figure 6(b), suggesting that the alignment of the vorticity vector with the intermediate strain rate is unaffected by the enstrophy production rate.

Figure 7 shows a joint *pdf* between the cosine of the alignment angle between the extensive strain rate ($\boldsymbol{e_1}$) and the "swirling eigenvector" ($\boldsymbol{v_r}$) and the intermediate strain rate (s_2) for weakly swirling regions, i.e. the local swirling strength is less than the mean value ($\lambda_{ci} < \bar{\lambda}_{ci}$). It can be seen from the figure that the most likely alignment angle cosine is 1 and the contours slope towards negative s_2. This implies that weakly swirling regions show a preferential alignment between the "swirling eigenvector" and the extensive strain rate, whilst also tending to be topologically "tube-forming" due to the fact that the intermediate strain rate has a tendency towards being negative (compressive).

SUMMARY AND DISCUSSION

The "fatter" positive tail of figure 3 suggests an overall preference for the term $\omega_i S_{ij}\omega_j$ to favour enstrophy production (vortex stretching) over vortex compression. This term is dependent upon the interaction between straining and rotation, with the alignment between the vorticity vector and

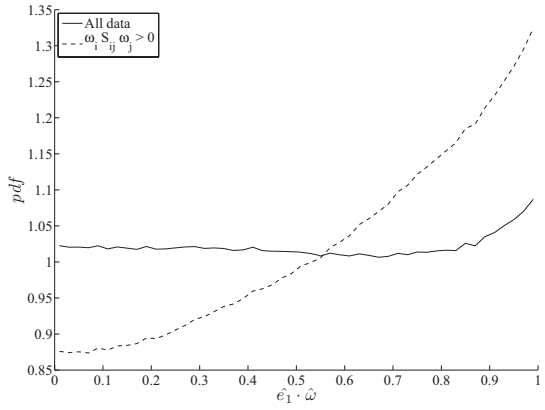

(a)

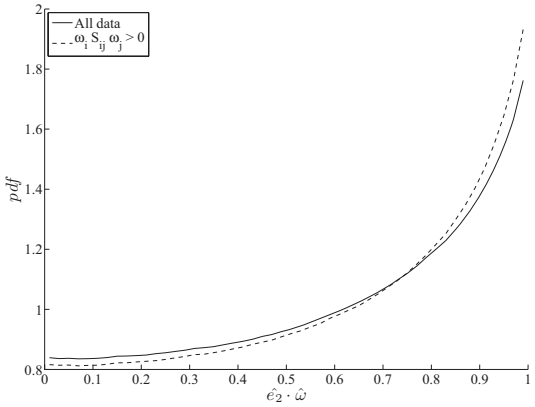

(b)

Figure 6: (a) Probability density function (*pdf*) of cosine of alignment angle between the unit vorticity vector ($\hat{\boldsymbol{\omega}}$) and the unit extensive strain rate eigenvector ($\hat{\boldsymbol{e_1}}$) for all data points and those for which the enstrophy production term ($\omega_i S_{ij} \omega_j$) is positive. (b) *pdf* of cosine of alignment angle between $\hat{\boldsymbol{\omega}}$ and the unit intermediate strain rate eigenvector ($\hat{\boldsymbol{e_2}}$) for all data points and those for which $\omega_i S_{ij} \omega_j$ is positive.

the strain rate tensor determining the size of the local enstrophy production rate. Figure 4 shows that a large proportion of the total volume of enstrophy producing regions within the turbulent flow are either weakly swirling ($\lambda_{ci} < \bar{\lambda}_{ci}$) or straining. However, these regions account for proportionately less of the overall total enstrophy production (even though 76.4 % of enstrophy producing regions are weakly swirling or straining, they only account for 41.3 % of the total enstrophy production rate). Strongly vortex stretching regions, which account for a greater proportion of the overall enstrophy production rate, are observed to be predominantly swirling regions with a high mean local swirling strength ($\lambda_{ci} > 2\bar{\lambda}_{ci}$). Regions of enstrophy production are also observed to be topologically "sheet-forming", due to the tendency of enstrophy forming regions to coincide with regions of positive (extensive) intermediate strain rate (s_2). Across all the data points, the vorticity vector has a tendency to align with the intermediate strain rate eigenvector whilst maintaining a random alignment with the extensive strain rate eigenvector. Figure 6(a) shows that in enstrophy producing regions the vorticity vector shows a preference to

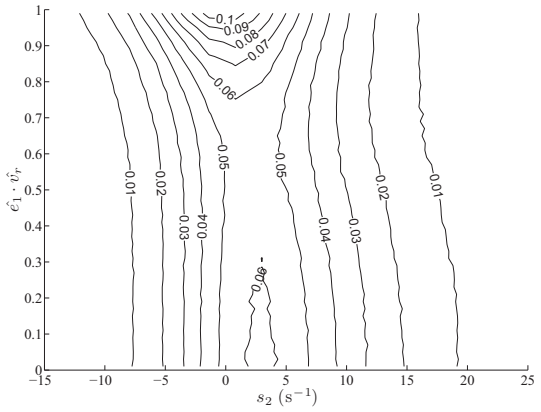

Figure 7: Joint probability density function between the cosine of the alignment angle between the extensive strain rate and the "swirling eigenvector" ($\hat{\boldsymbol{e_1}} \cdot \hat{\boldsymbol{v_r}}$), and the intermediate strain rate (s_2) for weakly swirling regions. These are defined as points at which the local swirling is less than the mean value, i.e. $\lambda ci < \bar{\lambda}_{ci}$.

align with the extensive strain rate eigenvector, indicated by the peak in the *pdf* at $\boldsymbol{e_1} \cdot \boldsymbol{\omega} = 1$.

Using this information it is possible to conjecture a mechanism whereby enstrophy is produced in a turbulent flow, and then subsequently evolved. It should be noted that this conjecture is based purely on kinematic, instantaneous PIV data that does not include dynamic information. The outline of this mechanism is presented in figure 8. In figure 8(a) energy is transferred from the mean flow into enstrophy. This occurs in regions in which the term $\omega_i S_{ij} \omega_j$ is positive, with a large proportion of this occurring in small, strongly vortex stretching regions. These enstrophy producing regions tend to be locally swirling, particularly those areas that possess a strong vortex stretching component. Additionally, the enstrophy production regions tend to be topologically "sheet-forming" due to the fact that the intermediate strain rate is positive. Within these enstrophy producing regions the vorticity vector tends to align to the extensive strain rate. It can thus be surmised that enstrophy producing regions tend, on average, to be weakly swirling "sheet-like" regions in which the vorticity vector is aligned to the extensive strain rate to a greater extent than enstrophy depleting regions.

Buxton and Ganapathisubramani (2009) showed that the "swirling eigenvector" ($\boldsymbol{v_r}$) preferentially aligns itself to the extensive strain rate eigenvector ($\boldsymbol{e_1}$) for all data points, as opposed to the vorticity vector which shows random alignment with $\boldsymbol{e_1}$ and preferential alignment with $\boldsymbol{e_2}$. This was found to be particularly the case for weakly swirling regions ($\lambda_{ci} < \bar{\lambda}_{ci}$). Figure 8(b) illustrates the evolution of a "sheet" of weakly swirling enstrophy under the action of an extensive strain rate. The "swirling eigenvector" ($\boldsymbol{v_r}$) of this weak "sheet" of vorticity is initially closely aligned to the extensive strain rate eigenvector, $\boldsymbol{e_1}$. Figure 7 shows that for weakly swirling regions, preferential alignment between $\boldsymbol{e_1}$ and $\boldsymbol{v_r}$ also coincide with regions of negative intermediate strain rate (s_2). The enstrophy of this weakly swirling "sheet-like" region is thus intensified by vortex stretching, due to the extensive strain rate acting upon the "swirling eigenvector". Simultaneously, the initial weakly swirling region is subjected to two compressive strain rates ($s_2 < 0$), hence will have a tendency to form "tube-like" topology. The ini-

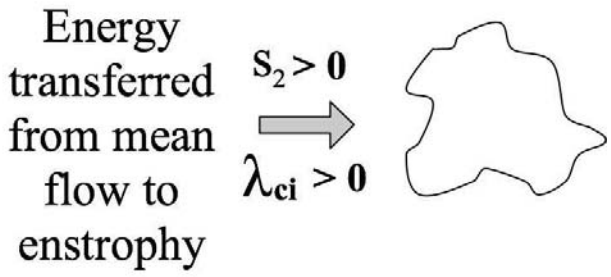

(a)

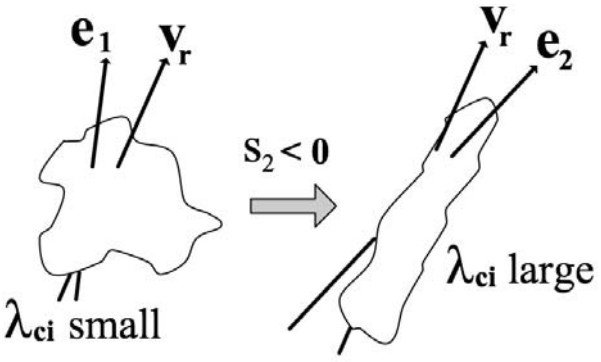

(b)

Figure 8: A cartoon depicting the suggested production and evolution of enstrophy (explanation in the text).

tially weakly swirling "sheet" will thus evolve into a strongly swirling (high enstrophy) "tube-like" structure. These high enstrophy "worms" have been reported in numerous studies, both numerically (Siggia 1983; Kerr *et al.* 1985; Jiménez et al., 1993 among various other studies) and experimentally (Ganapathisubramani et al., 2008), and have been shown to have characteristic diameters of the order 10η, where η is the Kolmogorov length scale.

REFERENCES

Ashurst, W. T.,Kerstein, A. R., Kerr, R. M. and Gibson, C. H., 1987, "Alignment of vorticity and scalar gradient with strain rate in simulated Navier-Stokes turbulence." *Phys. Fluids*, Vol. 30, pp. 2343-2353

Buxton, O. R. H. and Ganapathisubramani, B., 2009, "The classification and composition of fine scale eddies in a turbulent jet." *In Proc.* 47$^{\text{th}}$ *AIAA Aerospace Sciences Meeting Including the New Horizons Forum and Aerospace Exposition*, 5 - 8 January 2009, Orlando, Florida, Paper No. AIAA-2009-592

da Silva, C. and Pereira, J. C. F., 2008, "Invariants of the velocity-gradient, rate-of-strain, and rate-of-rotation tensors across the turbulent/nonturbulent interface in jets." *Phys. Fluids*, Vol. 20(055101), pp. 1-18.

Ganapathisubramani, B., Lakshminarasimhan, K. and Clemens, N. T., 2007, "Determination of complete velocity gradient tensor by using cinematographic stereoscopic PIV in a turbulent jet." *Exp. Fluids*, Vol. 42, pp. 923-939.

Ganapathisubramani, B., Lakshminarasimhan, K., and Clemens, N. T., 2008, "Investigation of three-dimensional structure of ne-scales in a turbulent jet by using cinematographic stereoscopic PIV." *J. Fluid Mech.*, Vol. 598, pp. 141-175.

Hamlington, P. E., Schumacher, J. and Dahm, W. J. A., 2008, "Direct assessment of vorticity alignment with local and nonlocal strain rates in turbulent flows." *Phys. Fluids*, Vol. 20(111703), pp. 1-4.

Hamman, C. W., Klewicki, J. C. and Kirby, R. M., 2008, "On the Lamb vector divergence in Navier-Stokes flows." *J. Fluid Mech.*, Vol. 610, pp. 261-284.

Jeong, J. and Hussain, F., 1995, "On the identification of a vortex." *J. Fluid Mech.*, Vol. 285, pp. 69-94.

Jiménez, J., Wray, A. A., Saffman, P. G. and Rogallo, R. S., 1993, "The structure of intense vorticity in isotropic turbulence." *J. Fluid Mech.*, Vol. 255, pp. 65-90.

Kerr, R. M., 1985, "Higher-order derivative correlations and the alignment of small-scale structures in isotropic numerical turbulence." *J. Fluid Mech.*, Vol. 153, pp. 31-58.

Mullin, J. A. and Dahm, W. J. A., 2006, "Dual-plane stereo particle image velocimetry measurements of velocity gradient tensor fields in turbulent shear flow II. Experimental results." *Phys. Fluids*, Vol. 18(035102), pp. 1-28.

She, Z. S., Jackson, E. and Orszang, S. A., 1990, "Intermittent vortex structures in homogeneous isotropic turbulence." *Nature*, Vol. 344,pp. 226-228.

Siggia, E.D., 1981, "Numerical study of small-scale intermittency in three-dimensional turbulence." *J. Fluid Mech.*, Vol. 107, pp. 375-406.

Sreenivasan, K. R. and Antonia, R. A., 1997, "The Phenomenology of Small-Scale Turbulence." *Annu. Rev. Fluid Mech.*, Vol. 29,pp. 435-472.

Tsinober, A., Kit, E. and Dracos, T., 1992, "Experimental investigation of the field of velocity gradients in turbulent flows." *J. Fluid Mech.*, Vol. 242, pp. 169-192.

Tsinober, A., Shtilman, L. and Vaisburd, H., 1997, "A study of properties of vortex stretching and enstrophy generation in numerical and laboratory turbulence." *Fluid Dyn. Res.*, Vol. 21, pp. 477-494.

Tsurikov, M., 2003, *Experimental investigation of the fine-scale structure in turbulent gas-phase jet flows.*, Ph.D Thesis, Department of Aerospace Engineering and Engineering Mechanics The University of Texas at Austin, USA.

Vincent, A. and Meneguzzi, M., 1991, "The spatial and statistical properties of homogenous turbulence." *J. Fluid Mech.*, Vol. 225, pp. 1-20.

Vincent, A. and Meneguzzi, M., 1994, "The dynamics of vorticity tubes in homogeneous turbulence." *J. Fluid Mech.*, Vol. 258, pp. 245-254.